第 48 卷 第 12 期
2021 年 12 月

湖南大学学报（自然科学版）
Journal of Hunan University (Natural Sciences)

Vol. 48 No. 12
December 2021

Theoretical Investigation of the Flexural Behavior of Concrete Beam Containing Internal Steel Plates

Douaa Najah*, Majid D. Mutasher

Civil Engineering Department, College of Engineering, University of Thi-Qar, Dhi-Qar, Iraq

Abstract: The main objective of this paper is to investigate the flexural behavior of simply supported RC beams strengthened internally with steel plates with three configurations. This investigation was done by using the ABAQUS program version 2017. The main parameter in this investigation was the configuration of steel plates (flat, curve, and round). For supporting Finite Element (FE_ results, four RC beams were cast with a rectangular cross-section of 200mm×150mm and a total length of 1200mm, one of these beams was a control beam, and three other beams were strengthened with 2mm steel plate with three different configurations (flat, curve and round). The experimental and numerical results showed that using steel plates as internal strengthening enhanced the load-carrying capacity for all tested beams, with a range of 15-24 % from the ultimate load of the reference beam. Furthermore, a specimen strengthened with a flat steel plate exhibited the highest increase in ultimate load. A parametric study was conducted to investigate the effect of concrete thickness and compressive strength, yield strength of steel plates, and the existence of a hole in steel plates.

Keywords: steel plate, flexural behavior, internal strengthening, finite element, ABAQUS.

内含钢板混凝土梁抗弯性能的理论研究

摘要：本文的主要目的是研究三种配置的钢板内部加固简支钢筋混凝土梁的弯曲行为。本次调查是使用
ABAQUS程序2017版完成的。本次调查的主要参数是钢板的配置（平面、曲线和圆形）。为支撑有限元结果，浇筑了四根截面为200毫米×150毫米、总长度为1200毫米的钢筋混凝土梁，其中一根梁为控制梁，另外三根梁采用2毫米钢板加固，具有三种不同的配置（平面、曲线和圆形）。实验和数值结果表明，使用钢板作为内部加固增强了所有测试梁的承载能力，范围为参考梁极限载荷的15-
24%。此外，用平板钢板加固的试样表现出最大的极限载荷增加。进行了参数化研究，以研究混凝土厚度和抗压强度、钢板的屈服强度以及钢板中是否存在孔洞的影响。

关键词: 钢板，弯曲性能，内部强化，有限元，ABAQUS。

1. Introduction

Improving the performance of the concrete members needs some techniques such as servicing and strengthening progress, recovering and increasing concrete strength and stiffness, refining of the concrete surface appearance, rising water tightness, preventing the use of corrosive materials for the reinforcement, and refinement the total durability of the concrete members [1]. Well-designed RC systems show excellent behavior through many decades. Nevertheless, many factors influence the RC structures that reduce the load-carrying capacity, principally the mechanical and environmental factors [2]. Moreover, only slight studies deal with the concept of steel plates reinforcement [3–5]. The effect of replacing the longitudinal reinforcement with an equivalent cross-

Received: August 11, 2021 / Revised: October 8, 2021 / Accepted: November 12, 2021 / Published: December 30, 2021

About the authors: Douaa Najah, Majid D. Mutasher, Civil Engineering Department, College of Engineering, University of Thi-Qar, Dhi-Qar, Iraq

Corresponding author Douaa Najah, hzda2015@gmail.com

sectional area of checker steel plates was studied in [6]. The test results concluded that each crack, yield, and ultimate loads of steel-plated beams were lower than the reference beams due to the higher rebar yield strength than steel plate. Also, the observation of beams at the failure stage increased the crack width and decreased the number of cracks.

On the other hand, ductility increased when the cross-sectional area of the steel plate was increased. The shear performance of RC wide beams was investigated experimentally on three-wide beams reinforced by vertical shear steel plates. The fourth beam with web reinforcement was considered a reference beam [7]. The flexure mode in failure had been restricted to allow for the shear failure mode in all specimens. The results show that the direction of the steel plates enhanced the shear capacity, and the use of transverse hollow steel plates improved the ductility and shear capacity. Also, the ultimate displacement was increased using transverse hollow steel plates and deflecting the longitudinal vertical hollow and solid steel plates. Bolt arrangement was studied in [8] to connect the steel plate with concrete for strengthening, with a single row and stagger rows of bolts to connect the plates with concrete. The study showed the effect of the arrangement modes. Also, the research objective was to know the effect of steel plates on flexural capacity, which is affected by the arrangement of bolts. ANSYS software was used as a finite element tool. In general, the results showed improved carrying capacity of beams by using steel plates. However, the stagger arrangement was the best mode for improving the load-carrying capacity, yield load, and ductility. The effect of some parameters on the strength and ductility behaviors of plate reinforced composite coupling beams was investigated depending on the nonlinear finite element model (FEM) [9]. The research parameters were the geometry of steel plates, the ratios of steel reinforcement in beams, and the ratio of span to depth. The results found that the ratio of span to depth controls the anchorage length of the steel plates, and the most effective ratio was about 2. The insufficient anchorage length of the plate resulted from beam stiffness and strength.

The literature stated that utilizing steel plates for external strengthening of RC beams improved their flexural strength. Moreover, the literature demonstrates that the shear performance of RC beams was significantly enhanced by using internal steel plates instead of stirrups. In general, to the author's knowledge, minimal research was conducted to investigate the flexural behavior of RC beams internally strengthening with steel plates. Thus, this study numerically investigated RC beam flexure behavior strengthened by steel plates using the ABAQUS program version 2017. In this study, nine RC beams were modeled, and the FE results were verified with the experimental results. Also, a parametric study has been conducted to investigate the effect of thickness of steel plates, compressive strength of concrete, yield strength of steel plates, and the existence of holes in steel plates.

2. FE Modeling

Figure 1 shows the details of primary and secondary reinforcement using nonlinear FEM by the ABAQUS program conducted in this study on four models.

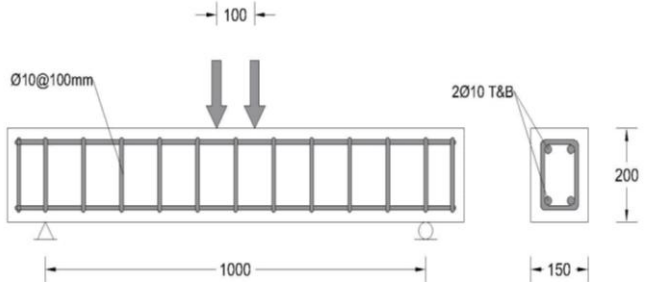

Fig. 1 Details of the reference beam

2.1. A Brief Introduction to the Testing

A reference beam and three strengthening beams with (2 mm) steel plate thickness, and three different configurations of steel plate were used to verify the accuracy of the finite element program. The geometry and strengthening details of specimens are shown in Figure 2. At 28 days of curing, the average compressive strength of concrete was 27 MPa. All properties of reinforcement and steel plates are shown in Tables 1 and 2, respectively. All specimens are tested under four-point bending with a maximum capacity of 150 kN. The clear span and distance between point loads are 1000 mm and 100 mm, respectively.

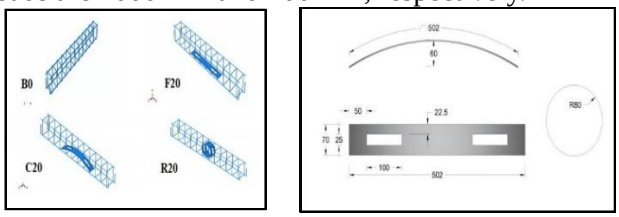

a) Details of the four specimens

b) Details of steel plates (all dimensions in mm)

Fig. 2 Geometries and strengthening details of specimens

Table 1 Properties of steel reinforcement bars

Type of steel	Diameter (mm)	Average yield stress (N//mm^2)	Average ultimate stress (N/mm^2)	Average Elongation (%)
Grade 60	10	590	800	12.33

Table 2 Yield and ultimate tensile strengths and elongations of steel plates

The thickness of the tested steel plate (mm)	Average of yield tensile strength (MPa)	Average of the ultimate tensile strength MPa)	% Elongation at ultimate stress
6	230	355	27
4	260	385	24
2	290	375	20.5

2.2 Numerical Modeling

2.2.1. Developing the Material Model Using Concrete Damaged Plasticity

It is well known that the behavior of concrete is brittle, but under stress reflection, the tensile cracks may be closing, so the broken parts are being converged. Subsequently, the best way to describe the behavior of concrete is damage models. Therefore, and because of the opposite behavior of concrete and steel, the reinforced concrete structures have complex behavior that is difficult to describe. Thus, the Concrete Damage Plasticity Model (CDP) is the best model to define concrete for all reasons above [10, 11]. This model is mostly very suitable for presenting the modes of failures that depend on compression crushing and tensile cracking [10]. The CDP model was designed in [12] and developed in [13]; it was the most popular model to simulate concrete in the ABAQUS program. CDP model is designed to handle applications whose materials were exposed to dynamic, monotonic, or cyclic loading. Therefore, it allows recovering the stiffness during load reflections [14]. As shown in Figure (3), the unloaded response of the concrete specimen appears to be attenuated because of the material damage or degradation of elastic stiffness. The damage variables ❑ dt, and d_c, represent the amount of damage or loss of strength (Figure 3). The values of these variables range from 0 to 1, where 0 refers to undamaged material, and 1 refers to total loss of strength [14].

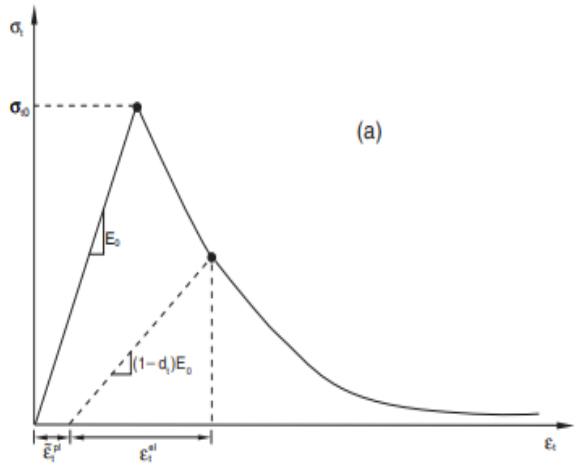

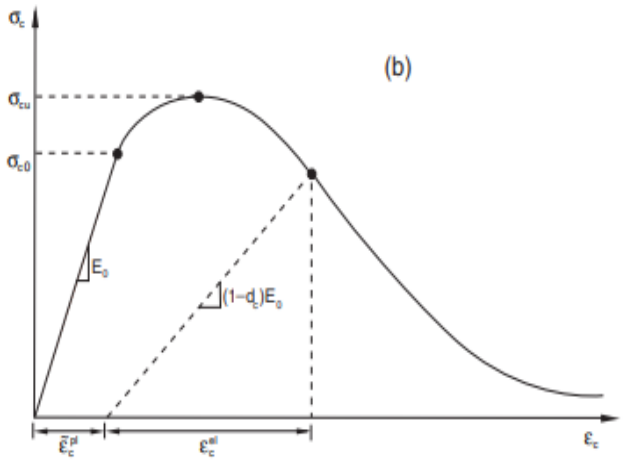

Fig. 3 Concrete response to uniaxial loading in (a) tension, (b) compression [14]

For compressive behavior, the definition of concrete material required the data of stress, inelastic strain, all equations used in the definition of concrete from the ABAQUS theory manual [14]. Inelastic or crushing strain is calculated according to Eq. 1.

$$\varepsilon_c^{\in ¿¿} = \varepsilon_c - \varepsilon_{0c}^{el} \quad (1)$$

where:

$$\varepsilon_{0c}^{el} = \sigma_c / E_0 \quad (2)$$

$\varepsilon_c^{\in ¿¿}$ - inelastic strain

ε_c - total strain

ε_{0c}^{el} - plastic strain

σ_c - the stress of concrete

E_0 - undamaged elastic modulus

In addition, the compression damage parameter is calculated as in Eq. 3.

$$d_c = 1 - \frac{\sigma_c}{\sigma_c^{max}} \quad (3)$$

for $\sigma_c \geq \sigma_c^{max}$, $d_c = 0$ for $\sigma_c < \sigma_c^{max}$

where:

d_c - damage parameter in compression.

On the other hand, the data for tension behavior and damage was calculated as in Equations 4, 5, and 6.

$$\varepsilon_t^{ck} = \varepsilon_t - \varepsilon_{0t}^{el} \quad (4)$$

$$\varepsilon_{0t}^{el} = \sigma_t / E_0 \quad (5)$$

$$d_t = 1 - \frac{\sigma_t}{\sigma_t^{max}} \quad (6)$$

where:

ε_t^{ck} - cracking strain;

d_t - damage parameter of tension.

Figure (4) shows the properties of concrete for compression and tension behavior utilized in the CDP model, where:

Dilation angle, ψ, is measured in the plane of p-q at confining pressure with a high level. The value depends on the study [15].

Flow potential eccentricity ε is a small positive value that defines the hyperbolic voltage ratio approached by its asymptote.

Stress ratio, f_{b0}/f_{c0}: is the ratio of the elementary equi-biaxial compression yield stresses to the elementary uniaxial compressive yield stress.

The second stress invariant, K, is the ratio of the invariants of second stress on the tension meridian to that on the compression meridian at an initial yield of any value of the pressure invariants.

Viscosity parameter, μ: As part of the CDP material behavior, the default value is zero in Abaqus/Standard, but it is not proper for nonlinear analysis. So it depends on the value from previous studies [16].

Table 3 Properties of concrete at elastic stage

Modulus of elasticity (MPa)	**Poisson's ratio**
15900	0.18 (assumed)

Table 4 Plastic parameters of concrete

Dilatation angle (degree)	**Eccentricity**	f_{b0}/f_{c0}	**K**	**Viscosity parameter**
37	0.1	1.16	0.667	0.0005

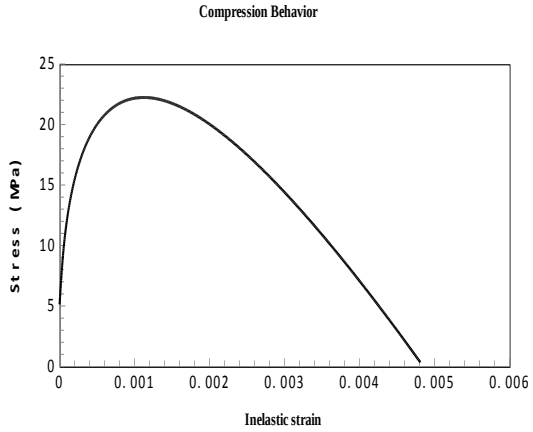

a)

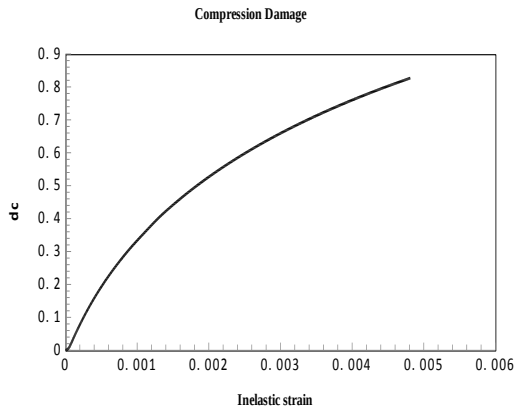

b)

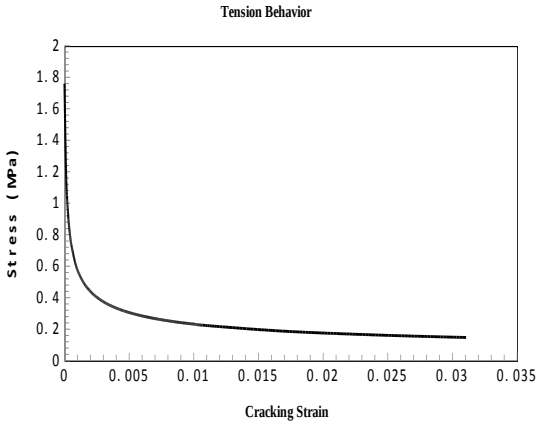

c)

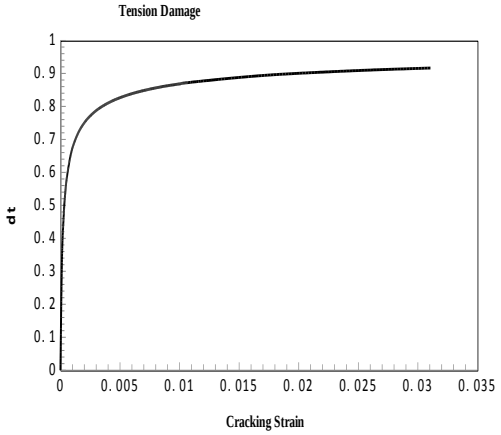

d)

Fig. 4 Properties of concrete in the CDP model: a: Compression behavior; b) Compression damage; c) Tension behavior: d) Tension damage

2.2.2. Steel

There are two stages to define the properties of the material of steel: elastic and plastic. For elastic behavior, specify the modulus of elasticity and Poisson's ratio as 200000MPa and 0.2, respectively. An engineering stress-strain curve usually illustrates the test of the tension of steel, so to define the steel in ABAQUS, the engineering stress-strain curve must be converted to a true curve according to Ramberg-Osgood theory (Figure 5) [17].

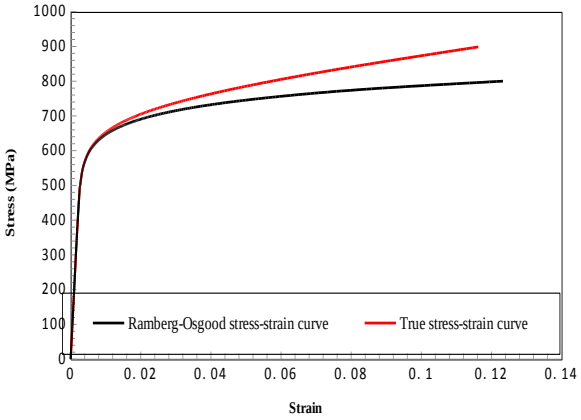

Fig. 5 Stress-strain curve of rebar

2.2.3 Parts, Assembly and Mesh Modules

Some partitions must be established to model the specimens. Therefore, all specimens consist of the following parts: the body of beam (concrete), longitudinal reinforcement (primary and secondary), transverse reinforcement (stirrups), bearing plate, and finally, the focus of this research is the steel plate in different configurations. Then, assembled these parts to form the complete model. Generally, in modeling the parts of specimens, there are two types of elements used: C3D8R: An 8- linear node brick, reduced integration, hourglass control; this element is used for solid parts (beam, bearing, and steel plates), T3D2: A 2-node linear 3-D truss, this one was utilized for all types of reinforcement. After defining all properties of the materials used in models, assemble parts to establish a model, and each model consists of one assembly. In finite element analysis, the accuracy of results depends on the size of the selected mesh. By the theory of FEM, a simulated model with a tiny mesh size gives accurate results but longer computational time [18]. There was a convergence study conducted to choose the appropriate mesh size, so the mesh size chosen was 15 mm in each part of the model. Figure 6 shows the mesh of assembly.

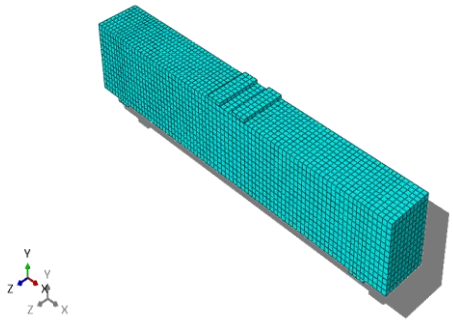

Fig. 6 Mesh of assembly

2.2.4 Boundary Condition and Details of Surface Interactions

The beams are supported simply; therefore, two support steel plates are modeled in a part module and given steel properties to simulate the supports. The original constraints are illustrated along the width of steel support, specifically on the partition line, as in Figure 7.

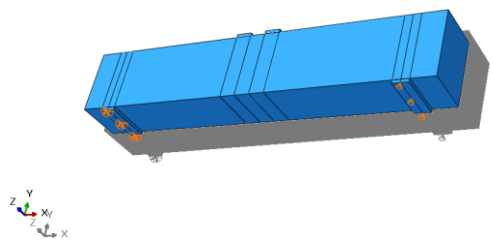

Fig. 7 Boundary condition

In ABAQUS, constraints permit modeling kinematic relationships between surfaces and points. The interaction module can define the contact between two surfaces and other functions [19]. This study used three types of constraints: embedded element**,** tie connection, and coupling interaction. The embedded element technique is used to assign a single or group of elements embedded into a host element group whose response will be utilized to constrain the translational DOFs of nodes of embedded elements. This technique is more appropriate to define the interaction between steel reinforcement and concrete, according to [11]. The tie constraints permit to merge of two regions together, although the created meshes on the surfaces of merged regions are different. A tie means connecting two discrete surfaces together. Therefore, there is no relative movement between them [19]. Coupling constraints mean that they couple the movement of a group of nodes on any surface to a movement of a reference node lying on the same surface [19]. In each model, a reference point should be constructed in the center of each bearing plate to be the loading point and used displacement control method by applying 50 mm translation in the y-direction of the reference points. This value is greater than the larger value of experimental tests. The displacement is applied through the analysis step. Compared with load control, the displacement control advantages are to overcome the convergence troubles and the modes of rigid body jointly, while a couple of bodies disconnected in connect pairs and obtain/follow the downward section of load-deflection and stress-strain curves [20].

3. Comparison Between Experimental and FE Results

3.1. Modes of Failure and Crack Pattern

The development of cracks represented the general modes of failure of all RC specimens. In flexural members, the crack develops when the tensile stresses in the extreme tension fiber exceed the modulus of rupture of concrete. Meanwhile, some micro flexural cracks started to appear early at the maximum positive bending moment region during the loading process. With overloading, these cracks were spread and widened, and then the diagonal cracks appeared at higher load. In all specimens, the failure began by yielding tensile steel reinforcement, and the crush of concrete in the compression zone was the final failure of all specimens.

Figure 8 shows the failure mode of all specimens. This figure noted that the flexure pattern failure is dominant for all beams except beam R20 that fail due to flexure and lack of bond pattern. There is a good agreement in crack patterns between experimental and numerical models concerning FEA. The results have concluded that the use of steel plates delayed the appearance of the initial crack, as shown in Table 5.

Table 5 Experimental and FE results

y	Experimental results								FE results		Exp. P_u / FE P_u
	Crack state		Yield state		Ultimate state		Failure state	% Increase in P_u			
	P_{cr} (kN)	δ_{cr} (mm)	P_y (kN)	δ_y (mm)	P_u (kN)	δ_u (mm)	δ_{max} (mm)		P_u (kN)	δ_{max} (mm)	
B0	9	0.509	51.538	3	61.894	10.179	10.37	-	62.542	9.215	0.989
F20	12	0.513	62.85	3.35	76.658	9.45	33.09	23.854	78.94	14.011	0.971
C20	11	1.05	61.16	3.9	74.6	9.391	30	20.53	77.14	15.302	0.967
R20	12	0.5	60.945	3.33	71.262	10	31.5	15.14	74.77	17.07	0.953

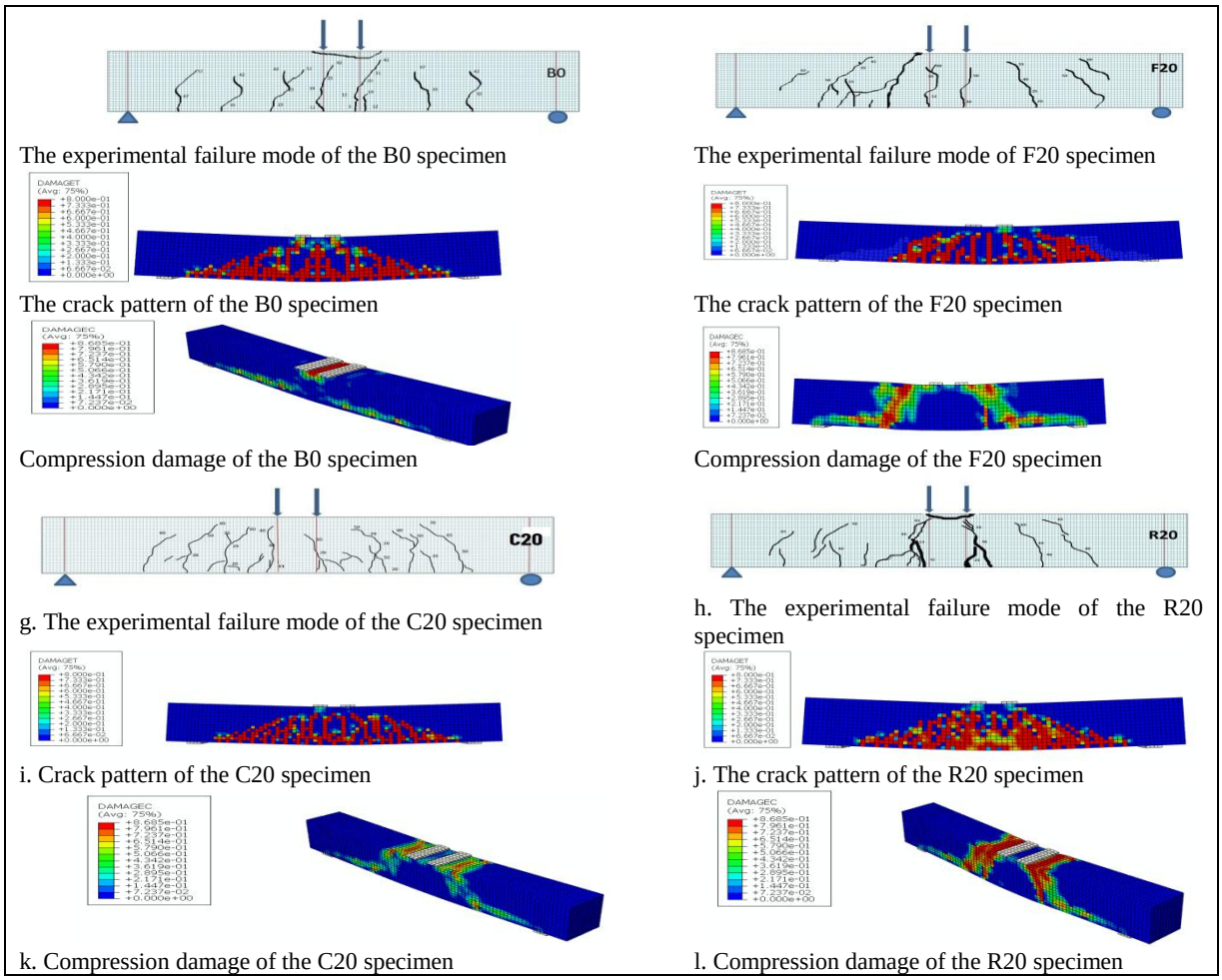

The experimental failure mode of the B0 specimen

The experimental failure mode of F20 specimen

The crack pattern of the B0 specimen

The crack pattern of the F20 specimen

Compression damage of the B0 specimen

Compression damage of the F20 specimen

g. The experimental failure mode of the C20 specimen

h. The experimental failure mode of the R20 specimen

i. Crack pattern of the C20 specimen

j. The crack pattern of the R20 specimen

k. Compression damage of the C20 specimen

l. Compression damage of the R20 specimen

Fig. 8 Failure modes of all specimens, experimentally and numerically

3.2. Load-Deflection Curves

The values of mid-span deflection versus load at the crack, yield, and ultimate stages had been obtained in Table 5. The test results showed that the yield and ultimate loads increased in all beams strengthened with steel plates. In addition, the increase of load-carrying capacity was ranged between 15-24 % from the ultimate load of the reference beam (B0). It was also noted that the highest increase in ultimate load for the F20 specimen was due to the configuration of the steel plate, which lies in the maximum positive moment zone. Figure 9 displays the experimental and FE load-deflection curves for all beams. Figure 9 demonstrates that the FE curves exhibited stiff behaviors after first cracking compared to the corresponding experimental curves. The reason is to disperse infinite freedom structure to limited freedom. This fact leads to an increase in load and decrease in deflection, which makes the FE curves ascend with more slope than experimental curves. Although all hints mentioned in [21] were considered, there was a difference between the experimental and FE results with a 4.7% as a maximum difference in ultimate load. The reason for the mismatch was that FE programs designed to analyze under perfect conditions are quite the opposite of what happens in real works. As stated before, the comparison between experimental and FE ultimate loads showed very close values with a maximum error of 4.7%. As a result, the proposed FE model will be used to conduct a parametric study on an effective

variable that might affect the flexural behavior of the strengthened beams.

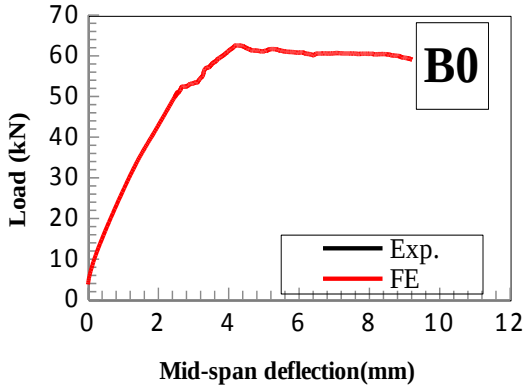

a. Load – deflection curves of B0

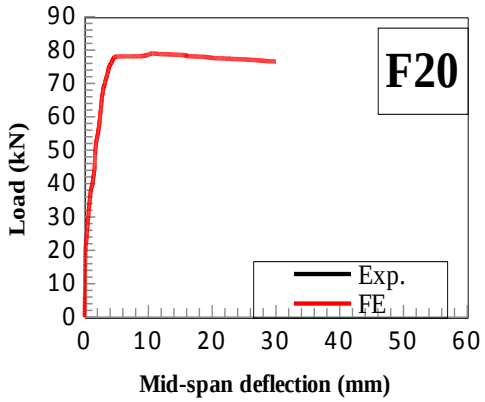

b. Load – deflection curves of F20

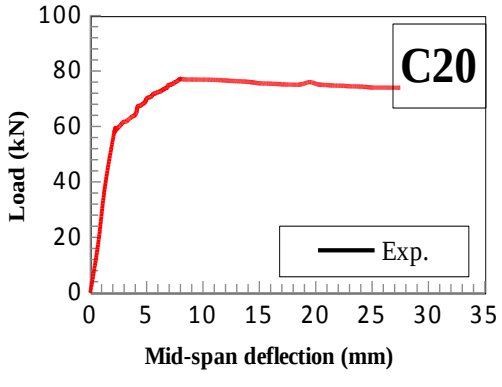

c. Load-deflection curves of C20

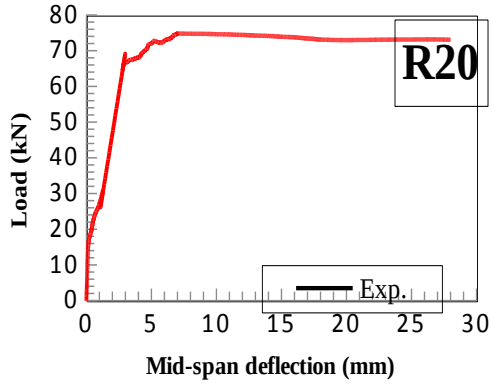

d. Load-deflection curves of R20

Fig. 9 Experimental and FE load-deflection curves of beams strengthened with steel plates

4. Parametric Study

4.1. Effect of Steel Plate Thickness

Each experimental specimen has been modeled with three steel plate thicknesses to investigate the effect of thickness on flexure capacity. Each steel plate has different properties for various thicknesses, as shown in Table 2. The numerical analysis results show that the flexural capacity was enhanced as thickness increased, but this concept does not apply to the round steel-plated models. In the stated models, the increase was slight because the plate does not fully utilize at the maximum bending moment. Since the yield stress for the 2mm thickness plate is higher than other thicknesses, the thickness does not work in current properties. Figure 10 shows the effect of steel plate thickness on load versus deflection curves at mid-span.

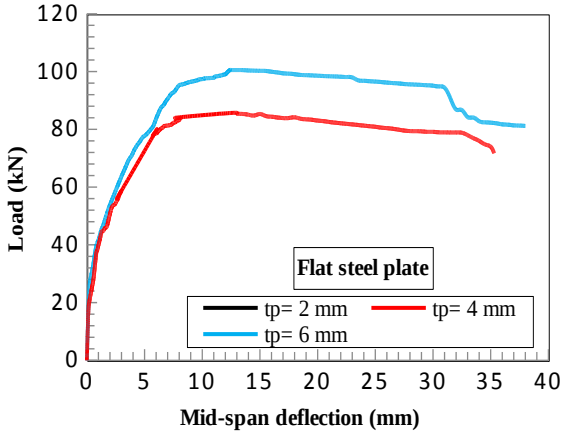

a. Load-deflection curves of flat steel-plated specimens

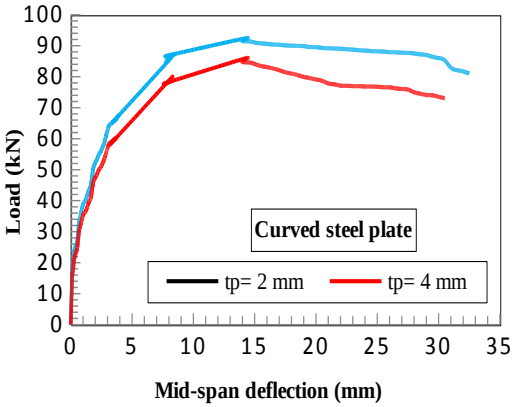

b. Load-deflection curves of curved steel-plated specimen

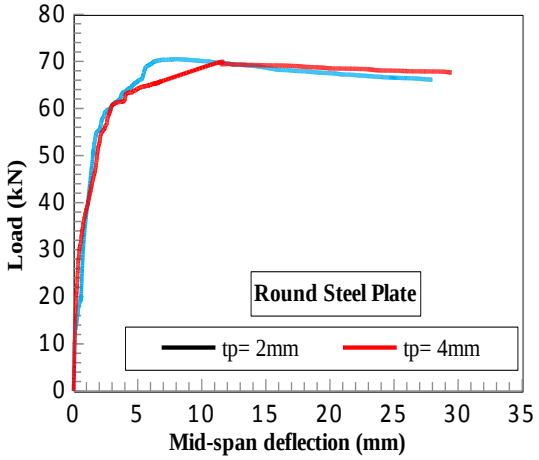

c. Load-deflection curves of round steel-plated specimens

Fig. 10 FE load-deflection curves for all models

4.2. Effect of Compressive Strength of Concrete

Three different compressive strengths of concrete (45 MPa, 60 MPa, and 75 MPa) have been considered to investigate the effect of compressive strength of concrete on the flexure behavior of RC beams which strengthened with different configurations of steel plate. From Figure (11), it was observed that the increase of compressive strength of concrete leads to an increase in ultimate load. Also, the curves behave stiffer with the increase of fc`, especially after 50 MPa. Finally, the stated figure revealed that the deflection was decreased with the increase of fc`, and specimens no longer resisted the applied load and failed in a brittle manner (i.e., after fc` = 50 MPa).

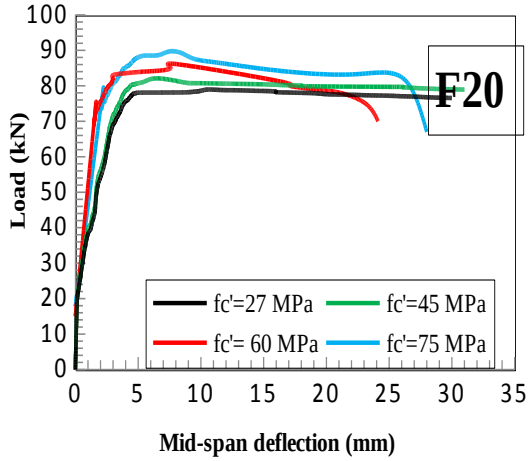

a. Load-deflection curves with different compressive strength of concrete of specimen F20

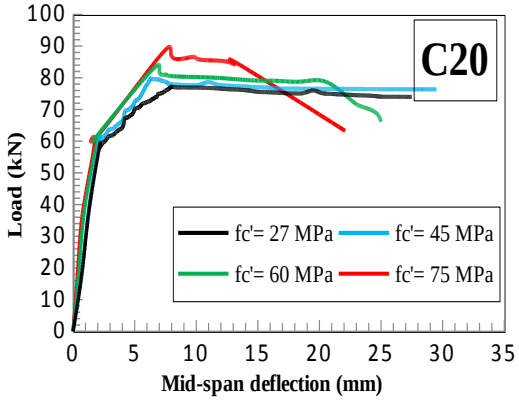

b. Load-deflection curve with different compressive strength of concrete of specimen C20

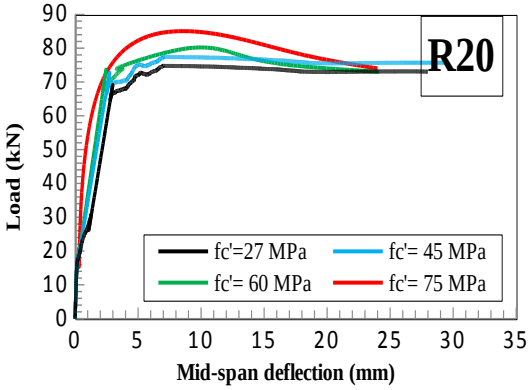

c. Load- deflection curve with different compressive strength of concrete of specimen R20

Fig. 11 Load-deflection curves with different compressive strengths of concrete

4.3. Effect of Yield Strength of Steel Plate

The effect of different yield strength levels of steel plates on flexure capacity was studied by considering three values (400 MPa, 500 MPa, and 600 MPa). Figure 12 concluded that the ultimate carrying capacity increased with the increase of yield strength of steel plates for all beams. Also, the deflection was decreased, but the slopes of curves and modes of failure were almost unchanged.

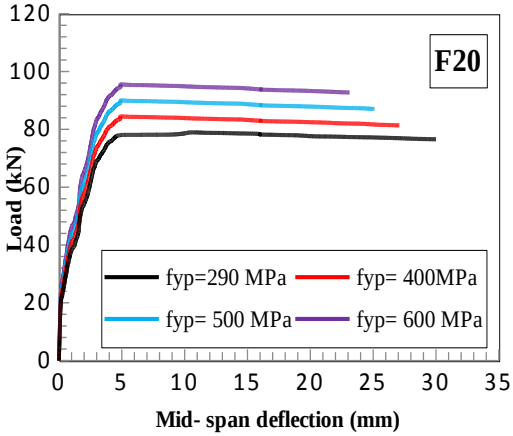

a. Load- deflection curves with the different yield strength of steel plate of specimen F20

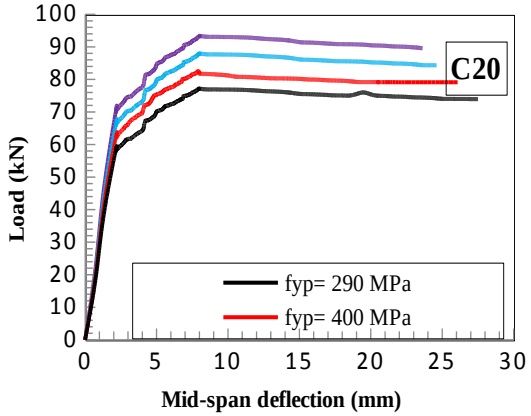

b. Load- deflection curve with the different yield strength of steel plate of specimen C20

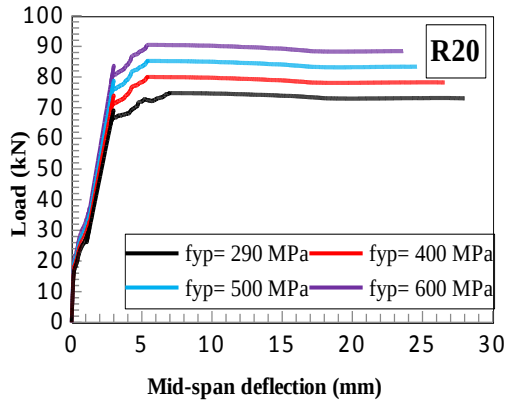

c. Load- deflection curve with the different yield strength of steel plate of specimen R20

Fig. 12 Load-deflection curves with the different yield strengths of steel plate

4.4. Effect of Holes in Steel Plates

The effect of holes in steel plates was investigated. The holes have been removed from steel plates in all specimens. Figure 13 shows that using solid steel plates decreased the flexure capacity of the strengthened beams because of a lack of interlock between steel plates and concrete, leading to a decrease in bond effect that reduced flexure capacity. On the other hand, the highest decrease in ultimate load has been recorded in the F20 specimen. The reason is that this configuration achieved the highest area of steel plate in the zone of maximum bending moment. Otherwise, the drop in ultimate load was slightly in C20 and almost negligible in R20 because of the previous reason.

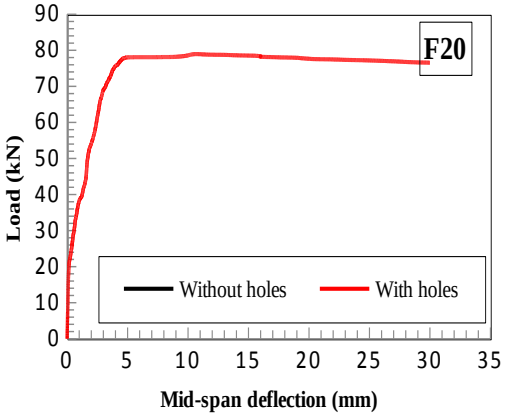

a. Load – deflection curves with two cases of existence of holes in steel plate of F20 specimen

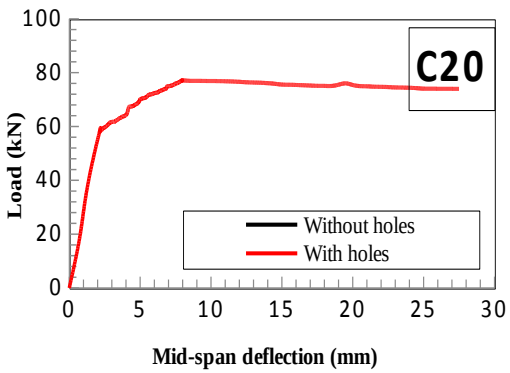

b. Load – deflection curves with two cases of existence of holes in steel plate of C20 specimen

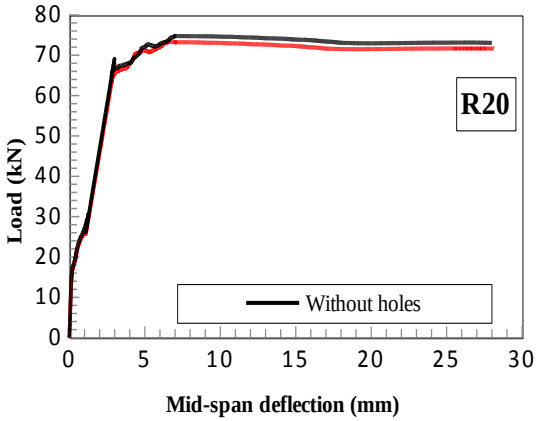

c. Load – deflection curves with two cases of existence of holes in steel plate of R20 specimen

Fig. 13 Load–deflection curves with two cases of holes in steel plate

5. Conclusion

The main objective of this paper is to investigate the flexural behavior of simply supported RC beams strengthened internally with a steel plate with three configurations. Each configuration has three thicknesses, and the FE program did this investigation. The following suggested conclusions can be noted from experimental and numerical results:

- Using steel plates enhanced the load-carrying capacity for all tested beams. The load-carrying

capacity increased between 15-24 % from the ultimate load of reference beam B0, and the highest increase in ultimate load was recorded for the F20 specimen.

- The effect of configuration on delaying the appearance of cracks has been approximately closed with values.
- From the results of numerical analysis, it noted that the flexural capacity enhanced as the thickness of the steel plate increased, except in round steel-plated models, the increase was slight.
- There is a good agreement between experimental and FE works with 4.7 % as a higher difference in ultimate load.
- The increase of compressive strength of concrete leads to an increase in ultimate load and deflection. Also, the modes of failure are almost unchanged.
- The ultimate carrying capacity increased with the increase of yield strength of steel plates. Also, the deflection was decreased, but the slopes of curves and modes of failure were almost unchanged.
- Beams containing steel plates with holes show higher ultimate loads than solid steel-plated beams, resulting from the improvement of the bond strength between the steel plate and concrete.

References

[1] BASHANDY A A. Flexural Strengthening of Reinforced Concrete Beams Using Valid Strengthening Techniques. *Archives of Civil and Mechanical Engineering*, 2013, 59(3): 275–292, doi: 10.2478/ace-2013-0015.

[2] RUDDOCK E C. Design of building frames. *Building and Environment*, 1978, 13(2): 145, doi: 10.1016/0360-1323(78)90034-3.

[3] SU R K L, LAM W Y, and PAM H J. Behavior of embedded steel plate in composite coupling beams. *Journal of Constructional Steel Research*, 2008, 64(10): 1112–1128.

[4] SU R K L, LAM W Y, and PAM H J. Experimental study of plate- reinforced composite deep coupling beams. *Structural Design of Tall and Special Buildings*, 2009, 18(3): 235–257.

[5] SUBEDI N K, and COYLE N R. Improving the strength of fully composite steel-concrete-steel beam elements by increased surface roughness—an experimental study. *Engineering Structures*, 2002, 24(10): 1349–1355.

[6] IBRAHIM K, MANSOR A A, NOMAN B J, et al. Effect of Replacing the Main Reinforcement by Sheet Steel Plate in Reinforced Concrete Beams. *Diyala Journal of Engineering Sciences*, 2021, 14(3): 141–151, https://doi.org/10.24237/djes.2021.14312.

[7] SALMAN W D. Effect of Steel Plates on Shear Strength of Wide Reinforced Concrete Beams. *Journal of Engineering and Development*, 2015, 19: 96–109.

[8] JAYAPRAKASH P O, SUDARSHAN P, and HEMALATHA C. Mechanical Properties of Strengthened RC Beams using Steel Plates. *International Journal of Innovative Technology and Exploring Engineering*, 2020, 9(4): 1208–1217, https://doi.org/10.35940/ijitee.d1444.049620.

[9] LAM WY, LI L, SU R K L, and PAM H J. Behavior of Plate Anchorage in Plate-Reinforced Composite Coupling Beams. *Hindawi Publishing Corporation, Scientific World Journal*, 2013: Article ID 190430, https://doi.org/10.1155/2013/190430

[10] ALFARAH B, LÓPEZ-ALMANSA F, and OLLER S. New methodology for calculating damage variables evolution in Plastic Damage Model for RC structures. *Engineering Structures*, 2017, 132: 70–86, https://doi.org/10.1016/j.engstruct.2016.11.022.

[11] RUSKA B, LAURSEN C B, and WICKSTRØM M, *Finite element modelling of reinforced concrete elements*. Aalborg University, Master Thesis, 2019, Available from https://projekter.aau.dk/projekter/files/307165023/Masters_thesis_BCM.pdf.

[12] LUBLINER J, OLIVER J, OLLER S, and ONATE E. A plastic-damage model for concrete. *International Journal of Solids and Structures*, 1989, 25(3): 299–326.

[13] LEE J, and FENVES G L. Plastic-damage model for cyclic loading of concrete structures. *Journal of Engineering Mechanics*, 1998, 124(8): 892–900.

[14] Abaqus 2016 . Abaqus 6.12 Theory Manual. 2016.

[15] SÜMER Y, and AKTAŞ M. Defining parameters for concrete damage plasticity model. *Challenge Journal of Structural Mechanics*, 2015, 1(3): 149–155, https://doi.org/10.20528/cjsmec.2015.07.023.

[16] DEMIR A, OZTURK H, EDIP K, et al. Effect of Viscosity Parameter on the Numerical Simulation of Reinforced Concrete Deep Beam Behavior. *Journal of Science and Technology*, 2018, 8(3): 50–56.

[17] PATWARDHAN P S, NALAVDE RA, and KUJAWSKI D. An Estimation of Ramberg-Osgood Constants for Materials with and without Luder's Strain Using Yield and Ultimate Strengths. *Procedia Structural Integrity*, 2019, 17: 750–757, https://doi.org/10.1016/j.prostr.2019.08.100.

[18] MORE S T, and BINDU R S. Effect of mesh size on finite element analysis of plate structure. *International Journal of Innovative Science Engineering and Technology*, 2015, 4(3): 181–185.

[19] HIBBITT, KARLSSON & SORENSEN, Inc ABAQUS/CAE User ' s Manual, 2001.

[20] OMRAN H Y, AND EL-HACHA R. Nonlinear 3D finite element modeling of RC beams strengthened with prestressed NSM-CFRP strips. *Construction and Building Materials*, 2012, 31: 74–85.

[21] BÄKER M. How to get meaningful and correct results from your finite element model. *arXiv Prepr. arXiv1811*. 2018, 05753: 1–26, Available FROM http://arxiv.org/abs/1811.05753.

参考文:

[1] BASHANDY A A. 使用有效加固技术对钢筋混凝土梁进行弯曲加固。土木与机械工程档案, 2013, 59(3): 275–292, https://doi.org/10.2478/ace-2013-0015.

[2] RUDDOCK E C. 建筑框架的设计。建筑与环境, 1978, 13(2): 145, doi: 10.1016/0360-1323(78)90034-3。

[3] SU R K L、LAM W Y 和 PAM H J. 复合连梁中预埋钢板的行为。钢结构研究杂志，2008，64（10）：1112-1128。

[4] SU R K L、LAM W Y 和 PAM H J. 板筋复合材料深连梁的实验研究。高层和特殊建筑的结构设计，2009，18（3）：235-257。
[5] SUBEDI N K 和 COYLE N R。通过增加表面粗糙度来提高全复合钢-混凝土-钢梁单元的强度——
一项实验研究。工程结构，2002，24（10）：1349-1355。
[6] IBRAHIM K、MANSOR A A、NOMAN B J 等人。钢筋混凝土梁用钢板代替主筋的效果。迪亚拉工程科学杂志, 2021, 14(3): 141–151, https://doi.org/10.24237/djes.2021.14312。
[7] SALMAN W D. 钢板对宽钢筋混凝土梁抗剪强度的影响。工程与发展杂志，2015，19：96-109。
[8] JAYAPRAKASH P O、SUDARSHAN P 和 HEMALATHA C. 使用钢板的强化钢筋混凝土梁的机械性能。国际创新技术与探索工程杂志, 2020, 9(4): 1208–1217, https://doi.org/10.35940/ijitee.d1444.049620.
[9] LAM WY、LI L、SU R K L 和 PAM H J. 板加固复合耦合梁中板锚固的行为。
兴达威出版公司，科学世界期刊，2013：文章 ID 190430，https://doi.org/10.1155/2013/190430
[10] ALFARAH B、LÓPEZ-ALMANSA F 和 OLLER S. 计算钢筋混凝土结构塑性损伤模型中损伤变量演变的新方法。工程结构，2017，132：70-86，https://doi.org/10.1016/j.engstruct.2016.11.022。
[11] RUSKA B、LAURSEN C B 和 WICKSTRØM M，钢筋混凝土构件的有限元建模。奥尔堡大学，硕士论文，2019年，可从 https://projekter.aau.dk/projekter/files/307165023/Masters_thesis_BCM.pdf 获得。
[12] LUBLINER J、OLIVER J、OLLER S 和 ONATE E. 混凝土的塑性损伤模型。国际固体与结构杂志，1989，25(3)：299–326。
[13] LEE J 和 FENVES G L. 混凝土结构循环载荷的塑性损伤模型。工程力学杂志，1998，124（8）：892-900。
[14] 巴库斯 2016。Abaqus 6.12 理论手册。 2016 年。
[15] SÜMER Y 和 AKTAŞ M. 定义混凝土损伤塑性模型的参数。结构力学挑战杂志，2015，1(3)：149–155，https://doi.org/10.20528/cjsmec.2015.07.023。
[16] DEMIR A、OZTURK H、EDIP K 等人。粘度参数对钢筋混凝土深梁行为数值模拟的影响。科技学报, 2018, 8(3): 50-56.
[17] PATWARDHAN P S、NALAVDE RA 和 KUJAWSKI D. 使用屈服强度和极限强度估算有和没有路德应变的材料的拉姆贝格-
奥斯古德常数。普罗西迪亚结构完整性，2019，17：750–757，https://doi.org/10.1016/j.prostr.2019.08.100。
[18] MORE S T 和 BINDU R S. 网格尺寸对板结构有限元分析的影响。国际创新科学工程与技术杂志, 2015, 4(3): 181–185.
[19] HIBBITT, KARLSSON 和 SORENSEN, 公司ABAQUS/CAE 用户手册，2001。
[20] OMRAN H Y 和 EL-HACHA R. 用预应力 NSM-碳纤维增强塑料条加固的钢筋混凝土梁的非线性3D有限元建模。建筑与建材，2012，31：74-85。
[21] BÄKER M. 如何从有限元模型中获得有意义且正确的结果。arXiv准备。arXiv1811。2018，05753：1-26，可从 http://arxiv.org/abs/1811.05753 获得。